44TH TURBOMACHINERY & 31ST PUMP SYMPOSIA
HOUSTON, TEXAS | SEPTEMBER 14 – 17 2015
GEORGE R. BROWN CONVENTION CENTER

DEVELOPMENT AND TESTING OF MULTI-STAGE INTERNALLY COOLED CENTRIFUGAL COMPRESSOR

J. Jeffrey Moore, Ph.D.
Manager, Rotating Machinery Dynamics
Southwest Research Institute®
San Antonio, Texas, USA

Neal Evans
Research Engineer
Southwest Research Institute®
San Antonio, Texas, USA

Jorge Pacheco, Ph.D.
Director Engineering Technologies and
Centrifugal Compressor Development
Dresser-Rand
Olean, New York, USA

Tim Allison, Ph.D.
Group Leader, Aeromechanics Group
Southwest Research Institute®
San Antonio, Texas, USA

Jason Kerth
Manager, Technology Commercialization
Dresser-Rand
Houston, Texas, USA

Dr. Jeffrey Moore is the manager of the Rotating Machinery Dynamics Section at Southwest Research Institute in San Antonio, TX. He holds a B.S., M.S., and Ph.D. in Mechanical Engineering from Texas A&M University. He has worked in positions related to centrifugal compressors and gas turbines at Solar Turbines Inc., Dresser-Rand, and Southwest Research Institute. He has authored over 30 technical papers related to turbomachinery and is a member of the Turbomachinery Symposium Advisory Committee, the IFToMM International Rotordynamics Conference Committee, and the API 616 and 684 Task Forces.

Neal Evans is a Research Engineer in the Mechanical Engineering Division at the Southwest Research Institute in San Antonio, TX. He received holds a B.S. in Multi-disciplinary Engineering from Purdue University and an M.S. in Acoustics from Penn State. He works in the area of acoustics and vibration, process analysis and design, and machinery development. Neal is a member of the ASME, Acoustical Society of America and Institute of Noise Control Engineering.

Dr. Tim Allison is the group leader of the Aeromechanics Group at Southwest Research Institute in San Antonio, TX, where his research interests include turbomachinery vibration analysis and testing, performance, blade dynamics, and rotordynamics. Dr. Allison received his M.S. in Aerospace Engineering from the University of Texas at Austin in 2005 and his Ph.D. in Mechanical Engineering from Virginia Polytechnic Institute and State University in 2007 with a focus on structural dynamics system identification.

Dr. Jorge Pacheco is the Director of Engineering Technologies and Centrifugal Compressor Development for Dresser-Rand in Olean, New York. He is responsible for the operational performance, strategic direction and development of the Aerodynamics-Rotordynamics, Materials-Solid Mechanics and Compressor Development teams. Dr. Pacheco received his B.S. degree in Mechanical Engineering from Universidad Simon Bolivar and Ph.D. degree from Carnegie Mellon University. Before joining Dresser-Rand, Dr. Pacheco was a professor at Universidad Simon Bolivar in the Thermodynamics and Transport Phenomena Department. Dr. Pacheco is a member of ASME.

Jason Kerth is a Technology Commercialization Manager for Dresser-Rand, focusing primarily on Compressed Air Energy Storage (CAES) products. Jason initially joined Dresser-Rand in 2005 as an application engineer providing centrifugal compressor application support for upstream and downstream oil and gas projects as well as various unique services including carbon dioxide compression for CCS, subsea compression, and high pressure acid gas compression. Prior to joining Dresser-Rand, Jason worked for ExxonMobil Upstream Research Company in design and evaluation of LNG facilities. Jason graduated from Texas A&M University with a B.S. and M.S. in Mechanical Engineering.

ABSTRACT

In order to reduce the amount of carbon dioxide (CO_2) released into the atmosphere, significant work has been completed to enable the capturing and storing of CO_2 from power plants and other major producers of greenhouse gas emissions. The compression of the captured carbon dioxide stream requires significant amounts of power, which impacts plant availability and operational costs. Preliminary analysis has estimated that the CO_2 compression process reduces typical power plant efficiency by 8% to 12%. The work presented in this paper supports the U.S. Department of Energy (DOE) National Energy Technology Laboratory (NETL) objectives of reducing the energy requirements for carbon capture and storage in electrical power production. The primary objective of this study is to boost the pressure of CO_2 to pipeline pressures with the minimum amount of energy required. Previous thermodynamic analysis identified optimum processes for pressure rise in both liquid and gaseous states. Isothermal compression is well known to reduce the power requirements by minimizing the temperature of the gas entering subsequent stages. Intercooling is typically accomplished using external gas coolers and integrally geared compressors. For large scale compression, use of straight through centrifugal compressors, similar to those used in oil and gas applications including LNG production, is preferred due to the robustness of the design. However, external intercooling between each stage is not feasible. The current research develops a multi-stage internally cooled compressor diaphragm that removes heat internal to the compressor and leverages the previous work on a single stage cooled diaphragm. Experimental demonstration of the design was performed on a full-scale 3 MW, 6-stage back-to-back centrifugal compressor operating in a closed loop test facility over a range of operating conditions. This work is a full scale implementation of the previous single-stage cooled diaphragm test program of Moore, et al. (2011). A multi-stage cooled diaphragm design was implemented in the current work and improvements to the mechanical strength and manufacturing process were made. Testing with a high speed torque-meter provides direct comparisons between adiabatic (no cooling) and with cooling configurations.

INTRODUCTION

In the effort to reduce the release of CO_2 greenhouse gases to the atmosphere, sequestration of CO_2 from Integrated Gasification Combined Cycle (IGCC), Oxy-Fuel, and Pulverized Coal (PC) power plants is being pursued. This approach, however, requires significant compression power to boost the pressure to typical pipeline levels. According to (Herzog, 1997), the power penalty for carbon capture can be as high as 27-37 percent for a traditional PC power plant and 13-17 percent for a typical IGCC plant. The compression represents a significant percentage of this total. The goal of this research is to reduce this penalty through novel compression concepts by developing concepts to boost the pressure of CO_2 to pipeline pressures with the minimal amount of energy required. Fundamental thermodynamics were studied to explore pressure rise in both liquid and gaseous states. In addition to compression options, liquefying CO_2 and liquid pumping were explored as well.

Isothermal compression can be accomplished with an integrally geared type of machine where multiple pinions are driven off of a common bull gear. Up to 10 stages of compression can be implemented with this arrangement. However, reliability of integrally geared compressors cannot match the in-line centrifugal machines that are widely used in the oil and gas industry. Therefore, this research seeks to design an internally cooled, in-line centrifugal compressor diaphragm that removes the heat of compression without the need for external intercoolers using liquid cooling. Significant challenges exist in cooling a high velocity gas internal to the compressor, such as limited surface area and minimizing pressure drop of the gas stream. By utilizing 3D Computational Fluid Dynamics analysis, an optimal design was achieved that provides good heat transfer while adding no additional pressure drop. A single-stage prototype diaphragm was built and tested to determine both aerodynamic and heat transfer performance (Moore, et al., 2011) under Phase II for a DOE-funded program.

Anticipated power savings from utilizing an internally cooled diaphragm were calculated and compared with conventional back-to-back compressors and with the power baseline for the DOE reference pulverized coal plant with carbon capture in Ramezan (2007):

- Single stream inlet Pressure/Temperature = 14.8 psia / 115°F
- Discharge Pressure = 2,150 psia
- Intercooler/After-cooler Exit Temperature = 115°F

The following configurations were analyzed for power comparisons:

1. DOE baseline (efficiencies and refrigeration/ liquefaction cycle performance calibrated to match data in [1])
2. Back-to-back LP and HP compressors with uncooled diaphragms
3. Back-to-back LP and HP compressors with cooled diaphragms, 15% effectiveness, 85°F cooling water
4. Back-to-back LP and HP compressors with cooled diaphragms, 20% effectiveness, 85°F cooling water

The power calculations in this analysis include gas horsepower for compression, cooling horsepower required for liquefaction, pumping horsepower, and gearbox power losses of 2%. The estimates exclude bearing and windage losses and power required for the pumping and chilling of cooling water.

The overall compression system analysis results for the methods shown above are displayed in Table 1. A back-to-back compressor with a cooled diaphragm is expected to achieve 10.4-11.7% power savings (15-20% effectiveness) relative to the DOE baseline case.

The goal of the current work was to develop and construct a pilot-scale demonstration compression plant to optimize CO_2 compression, as well as perform a balance of plant measurement for total power required and savings realized by

improving on the technology developed in Phase II, but in a multi-stage version of the cooled diaphragm design. A new compressor, based on a Dresser-Rand DATUM® D12 frame size, consisted of a six-stage, back-to-back centrifugal compressor (D12R6B) that incorporated the cooled diaphragms. A new test loop with required coolers, valves, and piping was constructed to test this new compressor. The cooled diaphragm, compressor, and loop design, commissioning, and testing will be discussed in this paper. The compressor impeller selection was made for an adiabatic compressor for the design point of 15 psia (1.03 bara) to 250 psia (17.2 bara) for a mass flow of 15.1 lbm/sec (6.85 kg/s). This flow is equivalent to the CO_2 produced by a 35 MW coal fired power plant. The design speed of the compressor is 11,403 rpm and is driven by a 3 MW electric motor through a speed increasing gearbox.

Table 1. Overall Compression Power Savings Analysis Results

Case Description	Assumed Heat Exch. Effectiveness	Power Savings
1. DOE Baseline	NA	0%
2. D-R B2B LP and HP Uncooled Diaphragm	0%	6.6%
3. D-R B2B LP and HP with Cooled Diaphragm	15%	10.4%
4. D-R B2B LP and HP with Cooled Diaphragm	20%	11.7%

COMPRESSOR DESIGN CONCEPT

This section describes the development of a proprietary internally-cooled compressor diaphragm that removes heat of compression between each impeller. Figure 1 shows the conceptual design where cooling flow (blue) is routed through the diaphragms adjacent to the gas flow path (red). The total temperature increases, due to the work input of the impeller, are reduced through the diaphragm flow path thereby reducing the temperature into the downstream stage. An efficient heat transfer mechanism is necessary to ensure that the compression process is nearly isothermal. Various heat transfer enhancement techniques have been reported in the open literature. A comprehensive literature survey was performed and the feasibility of those reported techniques was assessed. Concepts of printed circuit heat exchangers were also adopted with the major difference being that the cooled diaphragm velocities are orders of magnitude higher and the aerodynamic flow path must be preserved.

COOLED DIAPHRAGM ANALYSIS

A reasonable performance estimate for the multi-stage compressor with internal cooling can be achieved using one-dimensional methods for both the coolant networks and the gas path. The approach requires a stage-by-stage performance estimate of the uncooled machine as a starting point, a definition of the cooling circuit geometry for each stage, and an estimate of the two-dimensional gas velocity profile through each diffuser and return channel. The methodology begins with the analysis of the cooling circuits. Each cooling circuit is subdivided into segments and a one-dimensional hydraulic network model is used to estimate the flow and pressure distribution through the segments. The size of the segments must be sufficiently small to support the assumptions that the temperature of the coolant does not change much over the length of a segment and the location of each segment can be characterized by a mean distance from the centerline of the machine.

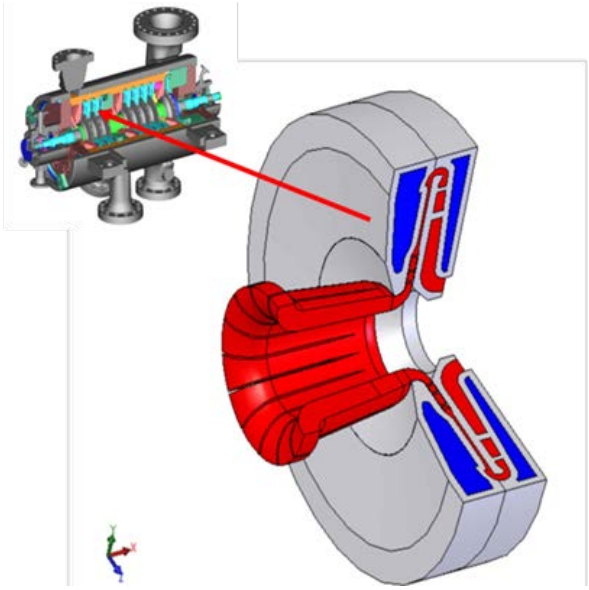

Figure 1. Cooled Diaphragm Concept

Given the coolant flow rates and channel dimensions throughout the network, coolant-side heat transfer coefficients can be determined using basic heat transfer relationships. The part of each coolant channel adjacent to the gas path is treated as the primary area and an extended surface model is used to characterize the effective contribution of the side walls of each coolant channel. Heat transfer from the back of the cooling channel has been ignored in modeling effort to date. While attempts were made in the cooling circuit design to maximize turning of the cooling fluid in order to enhance heat transfer, the modeling to date has not taken rigorous account of this effect. For both of these reasons, the basic model should tend to under-predict the heat transfer performance.

The main difficulty in realizing a one-dimensional model is characterizing the heat transfer on the gas side. The heat transfer coefficient clearly is not constant along the length of the gas path given that the velocity of the fluid is changing as well as the cross-sectional area of the channel. Algebraic manipulation of the basic Reynolds Number definition can be used to establish the following useful correlation for gas flow through a conical annulus. Conveniently, this correlation is independent of the angular orientation of the annulus relative to the centerline. Also, the thermodynamic condition of the gas does not enter the equation other than through the viscosity. The correlation accounts for the division of the annulus into

multiple passages in the longitudinal direction.

$$Re = \frac{\dot{m}}{\mu \cos\emptyset\left(fr\,\pi R_{mean} + \frac{Nv\,w}{2}\right)} \quad (1)$$

This Reynolds Number can be calculated at a series of locations along the diffuser and return channel passage, and used again with basic heat transfer relationships to determine the gas side heat transfer coefficient. According to this method, the gas-side heat transfer coefficient is highest at the entrance to the diffuser where the gas flow is fast and highly tangential. It diminishes through the diffuser and remains at a relatively low and consistent value through the return channel. Also, the heat transfer coefficient generally improves as the gas proceeds though a multi-impeller compression section, since the mass remains constant while the passage width becomes smaller. Inclusion of an appropriate model for the thermal entrance effect for each stage brought the results of the heat transfer prediction into very reasonable agreement with a CFD prediction that was also made.

Given the heat transfer coefficients, effective areas, thickness and conductivity of the metal separating the gas from the coolant, an overall heat transfer coefficient can be estimated linking each segment on the coolant side to each partition of the gas path. Given these overall heat transfer coefficients, the heat transfer through each linkage can be determined by the basic heat transfer relationship:

$$\dot{Q} = UA\Delta T \quad (2)$$

An enthalpy balance is still needed to relate the heat transfer magnitudes to the temperatures of the gas and the coolant in each segment of their respective paths. The interlinking of the heat transfer magnitudes with the temperature profiles makes the problem recursive, requiring an iterative solution. Furthermore, each stage in sequence depends on the outcome of the last.

In modeling work to date, no attempt has been made to adjust the stage-by-stage efficiencies in response to the change in volume flow or velocity, nor has any modification to the stage pressure ratios been considered. Instead, each stage is assumed to operate with the same efficiency and to produce the same pressure ratio as it would in the uncooled analysis. Therefore, the calculated change in total power stems only from the reduction in necessary head to achieve the same pressure ratio with the cooled arrangement.

COOLING WATER AND SYSTEM ANALYSIS

This section considers the impact of cooled compressor internals to the performance of the broader cooling system. The analysis that follows assumes that the two-section compressor system includes water-cooled heat exchangers to remove heat of compression after each compressor section in both the "Cooled" and "Uncooled" scenarios. Further, it is assumed in this example case that the cooling water circulated to the compressor diaphragms is the same water circulated to the external exchangers. The diaphragm cooling circuits applied in the test vehicle did require a higher pressure differential to circulate the desired amount of coolant than might be typically applied with conventional heat exchange equipment. Therefore, this analysis assumes that a booster pump is applied to elevate the pressure of cooling water from the supply pressure level required for the external exchangers to the supply pressure level required for the diaphragms. Alternatively, a completely closed-loop system for the diaphragms could be considered with a water-to-water heat exchanger, but this would add some additional pumping losses as well as diminish the overall performance improvement on account of the temperature approach of the additional heat exchanger. In the test program, a single pressure level system was used for simplicity, so the estimates here are predictions only.

An important point to realize when internal compressor cooling is considered is that the total cooling load of the system actually decreases. Since less power is being input into the system (via the motor), an overall energy balance of the system dictates that less heat needs to be rejected. Cooling duty is merely shifting from the external coolers to the internal cooled componentry. The analysis here assumes that the same target temperature rise of the cooling water is maintained in the external coolers, such that the water flow rate for these coolers can be reduced in proportion to the cooling duty. The pump power for the total circulating water and for the diaphragm coolant booster pump are calculated based on reasonable pressure differential assumptions and consistent efficiency assumptions. Then the pump powers are added to the compressor driver power in order to compare the overall system electricity consumption. These results are presented on a normalized basis in Table 2 for the design point. In each category, the normalized "Cooled" parameter has been normalized by the overall category figure for the "Uncooled" configuration. The net cooling water pumping reduces the power savings by 0.5% due to an increase in the total flow rate.

Table 2. Cooling Water Power Requirements

	Uncooled	Cooled
Driver Input Electric Power	**100.0%**	**97.1%**
Cooling Water Flows	**100.0%**	**114.1%**
Diaphragm Coolant Flow	N/A	40.5%
Ext. Heat Exchanger Coolant Flow	100.0%	73.5%
Total Pump Power	**100.0%**	**148.8%**
Diaphragm Water Booster Pump	N/A	34.7%
Utility Water Circulating Pump	100.0%	114.1%
Total Electrical Power	**100.0%**	**97.6%**
Total Cooling Duty	**100.0%**	**96.2%**
Diaphragm Heat Duty	N/A	22.6%
External Cooler Duty	100.0%	73.5%

COMPRESSOR LOOP DESIGN

A detailed design of the flow loop including heat exchanger location was developed, as represented by the solid

model in Figure 2. The compressor used up-connections and the required upstream lengths for performance measurements were maintained per ASME PTC-10. A thermal stress analysis and load study was performed for the CO_2 sequestration and compressor test loop using Intergraph Caesar II. Caesar II allows the user to input a series of pipes or structural steel members, modeled as beam elements, and define specific operating conditions for the system. The software computes displacements, loads, and stresses based on the user-defined inputs and compares these results to a database of codes and standards. Piping was modeled using ASTM A106B steel pipe according to ASME pipe code B31.3 for process piping. Compressor nozzle allowable loads were computed in accordance with API 617. Pipe supports were used to support weight loads, constrain motion due to thermal expansion, and to control low frequency vibration. A steady-state flow analysis of the test loop was run using the Stoner Pipeline Simulator (SPS) to simulate flow velocities, pressure drop, compressor performance, and valve operations.

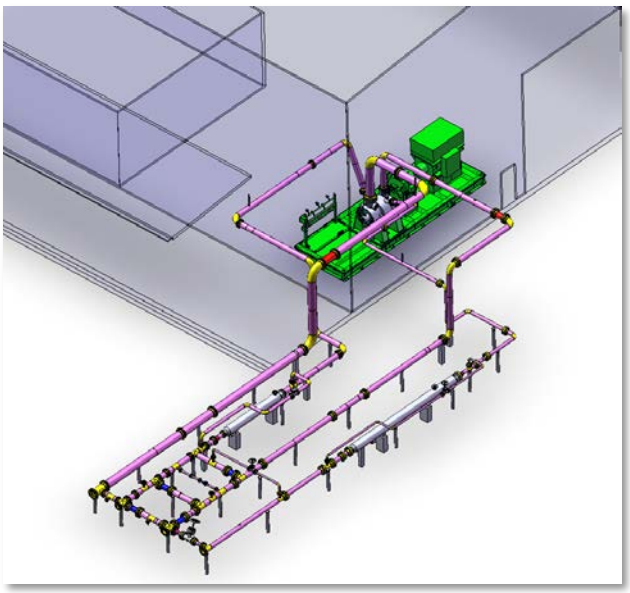

Figure 2. DATUM® Compressor and Test Loop Design

COMPRESSOR LOOP ASSEMBLY AND COMMISSIONING

The compressor package was delivered and set, leveled, and bolted to 20 sub-sole plates (Figure 3). The lube oil skid and rundown tank were moved into place and oil pipe connections were completed. The lube oil console was filled with ISO32 turbine oil and a lube oil flush was completed to ensure the cleanliness of the system before operation. All electrical connections between the variable frequency drive (VFD) and motor were completed, and the motor was successfully tested uncoupled from the gearbox and compressor. Final alignment and connection of the motor and gearbox was then completed. Field welds of large piping were made and alignment verified.

Hand valves, control valves, orifice plates, flow conditioners, strainers, and the cooling tower were received and installed. The heat exchangers and piping were assembled and the cooling water supply was tested through the process heat exchangers. The completed pipe assembly is shown in Figure 4. The piping and hand valves permit operation of the two compressor sections in series, parallel, and independent operation (with interconnecting pipes to maintain common pressures). This arrangement gives maximum flexibility when testing a back-to-back compressor. CO_2 is supplied from a liquid storage tank through a vaporizer and control valve. A venting control valve is also used to maintain the desired suction pressure to the compressor. Cooling water was provided to the heat exchangers and compressor diaphragm via an 800 gpm evaporative cooling tower. The flow to each diaphragm can be adjusted with individual hand valves and flow meters.

Figure 3. Installed Dresser-Rand DATUM® Compressor Package

The compressor package and pipe loop were commissioned, including oil flush, pipe alignment, shaft alignment, and mechanical testing. All mechanical parameters of the compressor met manufacturer's specifications. A trim balancing on the high-speed coupling on the gearbox end was performed to reduce the vibration to acceptable levels. Some speed control issues with the electric motor VFD were resolved and inaccurate readings from the torque meter were corrected. Some rework of the cooling water piping was required.

DATA ACQUISITION AND INSTRUMENTATION

A comprehensive channel list was identified that encompassed all instrumentation for purposes of machinery health monitoring, performance measurement, and loop control. This list included loop measurements, condition monitoring, vibration monitoring, and compressor diaphragm/cooling water measurements. Data acquisition and control were achieved with a custom developed interface including speed control, compressor throttling, loop inventory management, and data capture. Critical monitoring of the compressor package was achieved using a Woodward Micronet system. The package is equipped with a high speed coupling, which permits direct measurement of shaft torque and compressor power, important when cooling water is introduced to the diaphragms since the adiabatic assumption for gas horsepower calculations no longer

applies. The torquemeter accuracy is 1% over the entire torque range. However, since a power savings is calculated by measuring the reduction in power over the baseline, bias errors will be canceled out and other errors are expected to be lower than 1% over the small span between baseline and cooled test points. The head, flow and efficiency measurement uncertainties are +/- 0.5%.

Figure 4. Pipe Loop Assembly Aerial View

Internal temperature and pressure measurement probes were located in the return channel for Stages 1-2, 2-3, 4-5, and 5-6. Temperature measurements were also taken at the IGVs for Stages 2, 3, and 5. The internal measurement locations are shown in an example compressor schematic in Figure 5. The temperatures immediately downstream of the impeller could not be measured directly during cooled tests, but was calculated based on the stage inlet temperature and assuming the same stage isentropic efficiency for matched operating points from the adiabatic test.

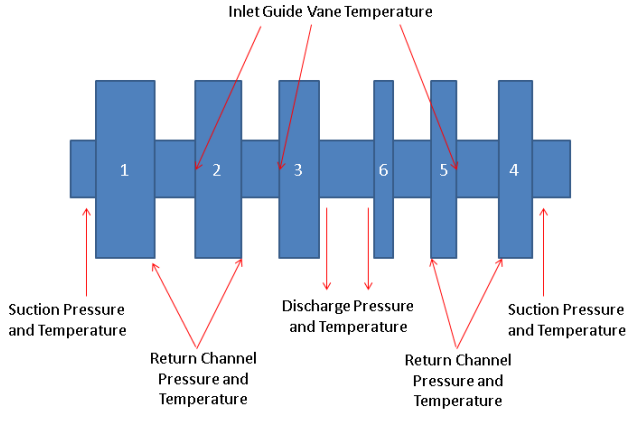

Figure 5. Locations of Internal Temperature Measurement Probes

COMPRESSOR PERFORMANCE CALCULATIONS

After the mass flow rates were determined, the temperature measurements at various locations inside the compressor were converted to total temperatures. The flow velocity at the suction and discharge measurement locations were used to calculate the total temperature and pressure at these locations using procedures based on those in ASME PTC-10, 1997, Section 5.4. This conversion procedure was also performed for temperature measurements at the impeller exit, diffuser vane exit, and return channel bend.

Total temperatures and pressures were used to calculate the actual head, polytropic head, and polytropic efficiency of each compressor section during adiabatic tests. First, the total enthalpy, $h_{t,suc}$, and entropy, s_{suc}, of the CO_2 at the suction flange were obtained using real gas properties from NIST REFPROP. The total discharge enthalpy, $h_{t,dis}$, and density, $\rho_{t,dis}$, at the discharge flange were also determined. Next, the isentropic discharge enthalpy, $h^*_{t,dis}$, and density, $\rho^*_{t,dis}$, were evaluated at the total discharge pressure and total suction entropy. Once these parameters were known, the actual head was calculated from

$$H^a = h_{t,dis} - h_{t,suc}, \tag{3}$$

the isentropic head was calculated from

$$H^* = h^*_{t,dis} - h_{t,suc}, \tag{4}$$

and the isentropic efficiency of the compressor is defined as:

$$\eta^* = \frac{H^*}{H^a}. \tag{5}$$

The polytropic performance of the compressor was calculated next. First, the isentropic exponent was defined as

$$k = \frac{ln\frac{P_{t,dis}}{P_{t,suc}}}{ln\frac{\rho^*_{t,dis}}{\rho_{t,suc}}} \tag{6}$$

and the polytropic exponent was defined as

$$n^P = \frac{ln\frac{P_{t,dis}}{P_{t,suc}}}{ln\frac{\rho_{t,dis}}{\rho_{t,suc}}}. \tag{7}$$

Next, the Schultz polytropic head correction factor was defined as:

$$f = \frac{H^*}{\left(\frac{k}{k-1}\right)\left(\frac{P_{t,dis}}{\rho^*_{t,dis}} - \frac{P_{t,suc}}{\rho_{t,suc}}\right)}. \tag{8}$$

Finally, the polytropic head was calculated from:

$$H^P = \left(\frac{n^P}{n^P - 1}\right)\left[\left(\frac{P_{t,dis}}{P_{t,suc}}\right)^{\frac{n^P-1}{n^P}} - 1\right] \times f \times \frac{P_{t,suc}}{\rho_{t,suc}} \tag{9}$$

and the polytropic efficiency was calculated from:

$$\eta^P = \frac{H^P}{H^a}. \tag{10}$$

The actual shaft power was calculated via speed and torque measurements on the shaft. The shaft power was equal to

$$TQHP = TQ \times N. \tag{11}$$

Horsepower savings from diaphragm cooling were calculated using the data gathered from the torque meter. These values were normalized by dividing by the average mass flow rate for each section as follows:

$$TQHP_{normalized} = \frac{TQHP}{m_{\dot{a}vg}} \quad (12)$$

Finally, the power savings at each operating point were calculated by comparing specific (normalized) horsepower for adiabatic and cooled tests:

$$Power\ Savings = \frac{TQHP_{adiabatic} - TQHP_{cooled}}{TQHP_{adiabatic}}. \quad (13)$$

Heat Exchanger Performance

The heat transfer effectiveness for each stage was calculated using the effectiveness-NTU method (Cengel, 2003), where dimensionless heat transfer effectiveness was defined as:

$$\varepsilon = \frac{\dot{Q}}{\dot{Q}_{max}} = \frac{Actual\ Heat\ Transfer\ Rate}{Maximum\ Possible\ Heat\ Transfer\ Rate} \quad (14)$$

In theory, the actual heat transfer rate can be computed from either the water or the CO_2 as

$$\dot{Q} = C_{H2O}\left(T_{H2O,out} - T_{H2O,in}\right) = C_{CO2}\left(T_{CO2,in} - T_{CO2,out}\right), \quad (15)$$

where $C_{H2O} = \dot{m}_{H2O}C_{p,H2O}$ and $C_{CO2} = \dot{m}_{CO2}C_{p,CO2}$ are the heat capacity rates of the cooling water and CO_2, respectively. The maximum heat transfer rate refers to the case when the CO_2 is cooled to the inlet temperature of the water and is defined as

$$\dot{Q}_{max} = C_{min}\left(T_{CO2,in} - T_{H2O,in}\right), \quad (16)$$

where C_{min} is the smaller heat capacity rate of the two fluids (in this case, C_{CO2} is always smaller than C_{H2O}).

In practice, however, water inlet and outlet temperatures were measured in supply and drain lines outside of the compressor casing and were lower and higher than the water temperature supplied locally to each diaphragm drain location due to heat transfer in the supply and drain lines within the compressor, so CO_2 properties were used for heat exchanger effectiveness calculations with $T_{CO2,in}$ equal to the impeller exit temperature and $T_{CO2,out}$ equal to the inlet guide vane (IGV) temperature for the next stage.

The impeller exit temperatures were not directly measured during testing, but in adiabatic testing the return channel/discharge flange temperatures were used instead to calculate the polytropic impeller efficiency for each stage. For cooled tests, the diaphragm inlet temperature was estimated using the measured pressure ratio and the same polytropic efficiency as the comparable adiabatic test point. Theoretically, the impeller efficiency should not differ for adiabatic and cooled tests.

Finally, no IGV temperature measurements were available for stage 6, so the stage 5-6 return channel temperature was used for both the stage 5 exit and stage 6 inlet temperatures during cooled testing. This simplification artificially decreases and increases the calculated stage 5 and 6 heat exchanger effectiveness, respectively.

COMPRESSOR TEST RESULTS

Several compressor operating configurations were tested in order to verify compressor performance and determine the effects of the cooled diaphragms. In the first configuration (Test 1), the sections were operated in series with independent throttle valves to operate over each section's entire design speed line. The adiabatic tests (with no cooling water) showed close correlation to the predicted aerodynamic performance maps. These tests established a baseline temperature distribution and power. The liquid cooling system was commissioned and tuned to provide the correct flow distribution to the diaphragms. The subsequent cooled diaphragm testing showed similar head-flow characteristic curves, but slightly higher head and pressure ratio for a given flow due to the increased volume reduction caused by lower stage discharge temperatures.

Subsequent testing (Test 2) matched overall pressure ratio and flow for multiple adiabatic and cooled operating points by adjusting throttle valve position and compressor speed. In this configuration, a single discharge throttle valve was employed for both sections. The data show that the cooled diaphragms reduce power consumption by 3-8% when the compressor is operated as a back-to-back unit, with the higher power savings at high flow operating points. At the design pressure ratio, the heat exchanger effectiveness and temperature drops for the cooled diaphragm were all slightly higher than predicted values but showed the same trends. A final test (Test 3) was performed with the same valve configuration as Test 2 but with no intercooler in order to mimic a straight-through compressor. During this test, speed was reduced to approximately 80% design speed in order to keep adiabatic test temperatures below compressor limits. Two data points were acquired during Test 3, the first point (A) matching pressure ratio and operating speed and the second point (B) matching pressure ratio and volume flow between the adiabatic and cooled tests.

The polytropic head for varying flow rates from Test 1 is plotted in Figures 6 and 7 for the two sections. The adiabatic test points are shown in blue, and the data points for testing with cooling water at the two different flow rates are shown in red and green. The solid black line denotes the predicted adiabatic curve. All data are normalized with respect to the adiabatic test data at the design flow.

The measured adiabatic data were reasonably close to the predicted adiabatic curve, with polytropic head for Sections 1 and 2 measured to be slightly lower and higher than predicted near the design point, respectively. The data also showed that diaphragm cooling changed the characteristics of the speed line slightly by increasing the volume flow capacity for each section, particularly near the choke side of the map. This performance change is attributed to the gas volume reduction that occurred as the gas was cooled in the diaphragm, which caused the latter stages in each section to stay out of choke and operate closer to their design point. The opposite would be true at low flow operation allowing the flow range to be extended by shutting off cooling flow when operating near the surge line.

Since the introduction of cooling water affected the head characteristics, the speed during the cooled tests was reduced to match identical discharge pressure as the adiabatic test in order to allow a direct comparison on power.

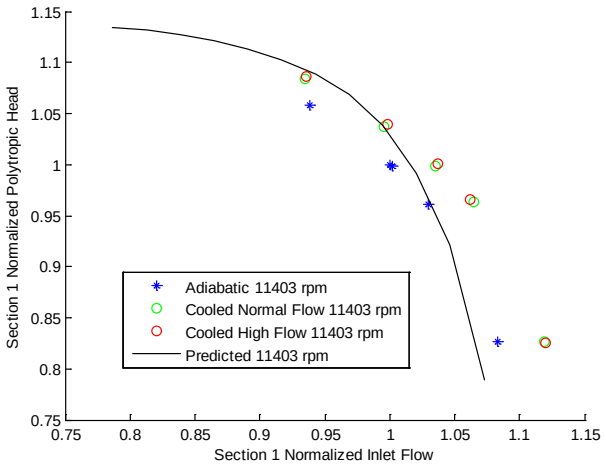

Figure 6. Section 1 Normalized Polytropic Head vs. Normalized Flow (Test 1)

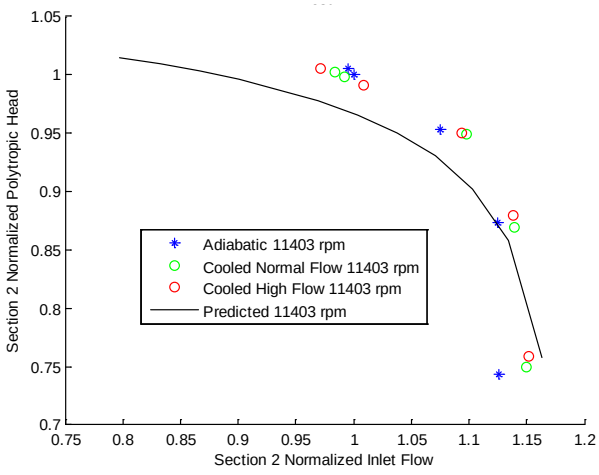

Figure 7. Section 2 Normalized Polytropic Head vs. Normalized Flow (Test 1)

Internal temperature measurements were taken at various points along the compressor. At each of these points, several temperature and pressure measurements were taken at different circumferential locations. These data points were averaged to get a temperature and pressure at each location. For both the adiabatic and cooled cases, the predicted design point temperature was plotted against the actual design point temperature in Figures 8 and 9 for Sections 1 and 2, respectively. These results indicate that the adiabatic temperature rise was slightly higher than predicted and cooled temperatures were slightly lower than predicted but showed good agreement overall. The measured discharge temperature was over 100°F lower for the cooled case.

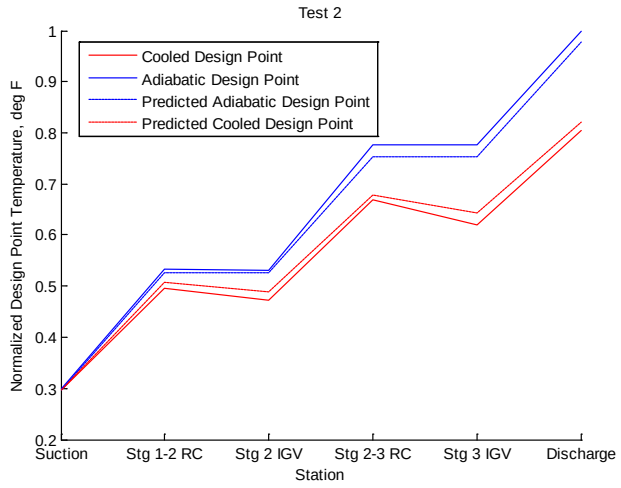

Figure 8. Section 1 Comparison with Predicted Normalized Temperature for Design Flow Conditions

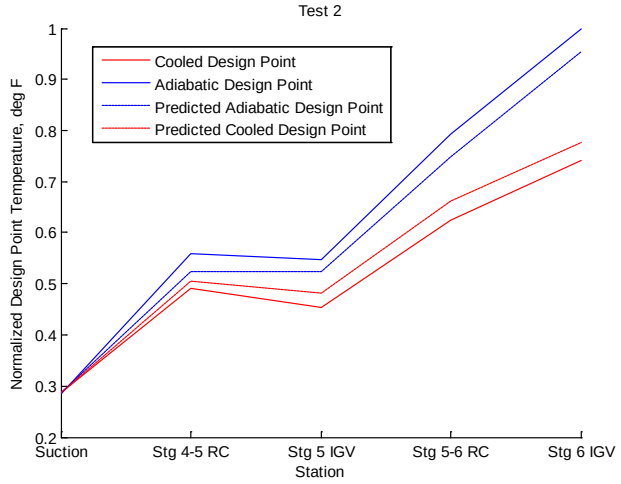

Figure 9. Section 2 Comparison with Predicted Normalized Temperature for Design Flow Conditions

The effectiveness of each stage vs. normalized flow rate is compared with the predicted effectiveness in Figure 10 for Test 2. As expected and noted previously, accuracy of the stage 5 and 6 heat exchanger effectiveness is reduced due to the lack of a stage 6 IGV temperature measurement, and results for these stages are significantly lower and higher than predictions, respectively. Stage 3 is the final stage for the 1st section, so heat transfer effectiveness in this stage is limited without a return channel (note that it is also unnecessary since last-stage cooling is accomplished through external coolers). The most accurate effectiveness measurements are taken from stages 1, 2, and 4 and show effectiveness slightly higher than predicted for all stages and ranging from 12-30% depending on operating point, stage, and intercooling configuration.

The measured horsepower savings for Test 2 are shown in Table 3. These results show that horsepower savings varies from 3% at low flows to 8% at high flows. The power savings at the design pressure ratio was calculated to be 3.2%, higher than the predicted power savings of 2.9%.

Table 3. Horsepower Percent Savings with Intercooler

Point	Adiabatic versus Cooled diaphragm difference (%)
1	8.0
2	6.3
3 (Design PR)	3.2 (Predicted 2.9%)
4	3.0
5	3.0
6	3.3

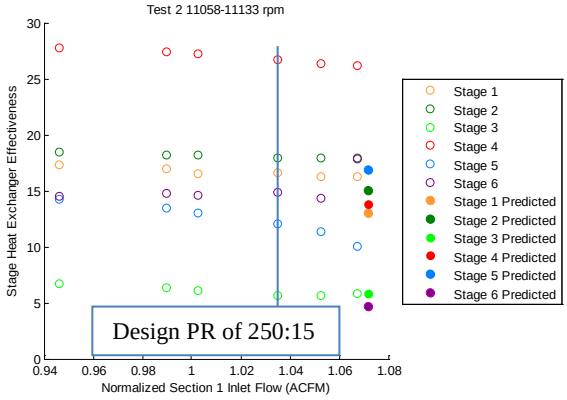

Figure 10. Heat Exchanger Effectiveness for CO_2 vs. Normalized Flow for Each Stage, Test 2

The results from Test 3 (no intercooling to simulate a straight-through compressor), as shown in Table 4, showed even higher power savings of 9% at the design point when matching pressure ratio and speed. Based on the trends seen in back-to-back testing, power savings are expected to be even higher at higher flows exceeding 10%.

Table 4. Horsepower Percent Savings with No Intercooler

Power Savings (%) A. Matching speed and pressure ratio	Power Savings (%) B. Matching flow and pressure ratio
5.6	9.0

CONCLUSIONS

All of the goals set forth in this test program have been accomplished. Aerodynamic testing of the compressor was completed with and without the cooling diaphragms activated and results showed that the cooled diaphragm technology reduces compressor power consumption by 3.0% near surge to 8.0% near choke when compared with the adiabatic case with intercooling between the two sections. Additional savings would result if the machine was configured as an 8-stage compressor, which would provide two additional internal heat exchangers. A 9.0% power savings was measured when the compressor was operated as a straight-through compressor with no intercooling at the design point and would be higher (>10%) at larger flows. The heat exchanger effectiveness for the cooled diaphragm was measured between 12-30%, depending on the stage, operating point, and back-to-back vs. straight-through intercooling configurations. The cooled diaphragms removed 75-100°F (28-35%) of the temperature rise within each section when compared to the adiabatic case. The measured temperature drop, heat exchanger effectiveness, and power savings were all slightly higher than predicted values. Operation of the cooled diaphragms changed the characteristics of the multi-stage machine, increasing flow capacity and pressure ratio compared to adiabatic performance at the same speed. Additional performance gains may be realized by designing the compressor aerodynamic flow path for the cooled case rather than the adiabatic case. No reliability issues associated with the cooled diaphragm design were encountered during testing including diaphragm leakage. While these results provided were for a CO_2 application, benefits can be realized for any high pressure ratio application or where reducing discharge temperatures is desired (e.g., preventing ethylene polymerization).

NOMENCLATURE

Symbols

ΔT	=	Temperature difference between the gas and coolant	(θ)
ε	=	Heat Exchanger Effectiveness	(-)
η	=	Isentropic Efficiency	(-)
ρ	=	Density	(ML^{-3})
A	=	Effective area	(L^2)
H, h	=	Head, Enthalpy	(L^2T^{-2})
f	=	Schultz Correction Factor	(-)
fr	=	Fraction of annular cross-sectional area that is not taken up by vanes	(-)
k	=	Isentropic Exponent	(-)
$\dot{m}$	=	Mass Flow	(MT^{-1})
n^P	=	Polytropic Exponent	(-)
N	=	Speed	(T^{-1})
Nv	=	Number of vanes in the annulus	(-)
P	=	Pressure	($ML^{-1}T^{-2}$)
$\dot{Q}$	=	Heat Transfer Rate	(ML^2T^{-3})
R_{mean}	=	Distance from the centerline of the machine to the mean middle of the passage cross-section.	(L)
s	=	Entropy	($L^2T^{-2}\theta^{-1}$)
T	=	Temperature	(θ)
$TQHP$	=	Torquemeter Horsepower	($ML^2\ T^{-1}$)
$\emptyset$	=	Angle between the streamline and the meridional direction	(Deg)
μ	=	dynamic viscosity	($MT^{-1}L^{-1}$)
U	=	Overall heat transfer coefficient	($MT^{-3}\ \theta^{-1}$)
w	=	width	(L)

Subscripts & Superscripts

a	=	Actual
avg	=	Average
dis	=	Discharge
p	=	Polytropic
suc	=	Suction
t	=	Total
$*$	=	Isentropic

REFERENCES

ASME, B31.3, 2002, Process Piping Design Standard, American Society of Mechanical Engineers, New York, NY.

ASME, PTC 10, 1997, Performance Test Code on Compressors and Exhausters, American Society of Mechanical Engineers, New York, NY.

Cengel, Y. A., 2003, "Heat Transfer: A Practical Approach," 2nd. Ed., McGraw-Hill, New York, NY, 2003

Herzog, H. J., 1997, "CO_2 Capture, Reuse, and Sequestration Technologies For Mitigating Global Climate Change," Advanced Coal-Based Power and Environmental Systems Conference, Pittsburgh, PA (United States), July 22-24, 1997.

Moore, J., Lerche, A., Delgado, H., Allison, T., Pacheco, J., 2011, "Development of Advanced Centrifugal Compressors and Pumps for Carbon Capture and Sequestration Applications", Proceedings of the Fortieth Turbomachinery Symposium, September 12-15, 2011, Houston, Texas

MPMS Chapter 14.3.4, 2002, Concentric, Square-edged Orifice Meters – Part 4 – Background, Development, Implementation Procedures and Subroutine Documentation, 3rd Edition, American Petroleum Institute, Washington, D.C.

NIST, 2007, NIST Reference Fluid Thermodynamic and Transport Properties - REFPROP, Version 8.0, Physical and Chemical Properties Division, National Institute of Standards and Technology (NIST), Boulder, Colorado 80305, April 2007.

Ramezan, et al., 2007, "Carbon Dioxide Capture from Existing Coal-Fired Power Plants," DOE/NETL-401-110907, National Energy Technology Laboratory, Nov. 2007.

Ridouane, E. H. and Campo, A., 2008, "Heat Transfer Enhancement of Air Flowing Across Grooved Channels: Joint Effects of Channel Height and Groove Depth," Journal of Heat Transfer, Vol. 130, February 2008.

ACKNOWLEDGEMENTS

The authors would like to thank the National Energy Technology Laboratory (NETL) within the U.S. Department of Energy for providing the majority of the funding for this work and Dresser-Rand and Southwest Research Institute for the additional co-funding required.